JOURNAL OF GEOPHYSICAL RESEARCH, VOL. 87, NO. B6, PAGES 4657–4667, JUNE 10, 1982

Lithospheric Flexure at Fracture Zones

DAVID SANDWELL[1] AND GERALD SCHUBERT

Department of Earth and Space Sciences, University of California, Los Angeles, California 90024

Bathymetric profiles across six major fracture zones (FZ's) in the North Pacific are used to demonstrate the absence of vertical slip on the fossil fault planes. The scarp heights on these FZ's are constant with age and equal to the initial vertical offsets at the ridge–transform fault–FZ intersections. Because of the frozen-in scarp and the differential subsidence of lithosphere far from the FZ, the lithosphere bends in the vicinity of the FZ. This flexure results in a characteristic ridge-trough topographic FZ signature. The flexural amplitude, which is the difference between the scarp height and the overall change in depth across the FZ, increases with age. Good fits to the bathymetric profiles across the Mendocino and Pioneer FZ's are obtained by modelling the topography as the flexure of a thin elastic plate with an age-dependent effective elastic thickness. Results of the modelling indicate that the base of the elastic lithosphere is approximately defined by the 450°C isotherm. Maximum bending stresses at FZ's are on the order of 100 MPa, substantially less than the stresses encountered at subduction zones. Because the Mendocino and Pioneer FZ's are separated by less than a flexural wavelength, they are elastically coupled.

INTRODUCTION

Flexure of the oceanic lithosphere is commonly observed in the bathymetry across subduction zones and around islands and large seamounts [*Turcotte*, 1979]. The trench and outer rise topography at a subduction zone is the flexural response of the elastic lithosphere to a vertical end load and bending moment applied at the trench axis [*Gunn*, 1937, 1947; *Hanks*, 1971; *Watts and Talwani*, 1974; *Caldwell et al.*, 1976; *Parsons and Molnar*, 1976]. The moat and outer rise topography surrounding many islands and seamounts is the flexural response of the elastic lithosphere to the isolated vertical load [*Gunn*, 1943; *Walcott*, 1970; *Watts and Cochran*, 1974; *Watts*, 1978]. The wavelength of the flexural topography is a function of the effective elastic thickness h_e of the lithosphere, while the amplitude of the flexure depends on both h_e and the applied bending moment or vertical load.

Recent flexure studies of subducting oceanic lithosphere and lithosphere loaded by the Hawaiian-Emperor chain have shown that the effective elastic thickness of the lithosphere is approximately proportional to $(\text{age})^{1/2}$ [*Watts*, 1978; *Caldwell and Turcotte*, 1979; *Watts et al.*, 1980; *Bodine et al.*, 1981]. This behavior basically reflects the age-dependent thermal structure of the lithosphere and the strong temperature dependence of the creep processes which tend to relieve flexural stresses. To a first approximation, the uppermost portion of the lithosphere has a viscous relaxation time that is greater than the age of the lithosphere, and it therefore exhibits elastic behavior; the lower portion of the lithosphere is hotter, less viscous, and relieves stresses on a much shorter time scale [*Caldwell and Turcotte*, 1979]. The division between the upper elastic and lower viscous portions of the lithosphere occurs at a temperature between 300° and 600°C according to *Watts et al.* [1980], while *Caldwell and Turcotte* [1979] suggest a temperature of 700°C.

In this paper we demonstrate that lithospheric flexure also occurs at an oceanic fracture zone (FZ) as a consequence of the difference in subsidence rates on either side of the FZ and the permanence of the initial bathymetric step across the FZ. Figure 1 illustrates why this flexure occurs. Initially a FZ separates newly created lithosphere (0 Myr) from older lithosphere (20 Myr) (see A-A′ in Figure 1). As these two segments of lithosphere move away from the ridge crest from A-A′ to B-B′, the depth far from the FZ on the younger lithospheric segment increases at a higher rate than the depth far from the FZ on the older segment [*Menard and Atwater*, 1969; *Delong et al.*, 1977; *Sibuet and Mascle*, 1978]. This effect is shown by the two subsidence curves in the middle of Figure 1. By the time the two segments have evolved to B-B′, the overall change in depth across the FZ, h_B, is less than the initial value h_A. We propose, however, that the FZ does not slip during its evolution. Therefore the height of the scarp at the fracture zone will remain at its initial value h_A. The lithosphere must flex to satisfy both of these requirements as shown in the lower portion of Figure 1. The amplitude of this flexure δ_B is the change in the differential subsidence from A to B, i.e., $h_A - h_B$. Further evolution from B to C increases the flexural amplitude to δ_C. The shape of this flexural topography depends upon the effective elastic thickness h_e of the lithosphere. Since h_e is proportional to $(\text{age})^{1/2}$, the flexure is asymmetric about the FZ with the younger lithosphere flexing at a shorter wavelength than the older lithosphere.

The major objectives of this study are to demonstrate that lithospheric flexure occurs across the Pioneer and Mendocino FZ's and that this flexural topography is a primary topographic expression at these FZ's. This is accomplished by modelling the flexure and comparing the predicted depths with five bathymetric profiles crossing the two FZ's at different ages. In addition, we show that the flexure model is consistent with bathymetric profiles crossing four other north Pacific FZ's, the Clipperton, Clarion, Molokai, and Murray FZ's. The model for computing the flexure utilizes a thin elastic plate overlying an incompressible fluid half space. The model also incorporates a temperature-dependent effective elastic thickness. The ages on each side of the FZ determine both the initial bathymetric step across the FZ

[1] Now at National Geodetic Survey, National Ocean Survey, NOAA, Rockville, Maryland 20852.

Paper number 2B0365.
0148-0227/82/002B-0365$05.00

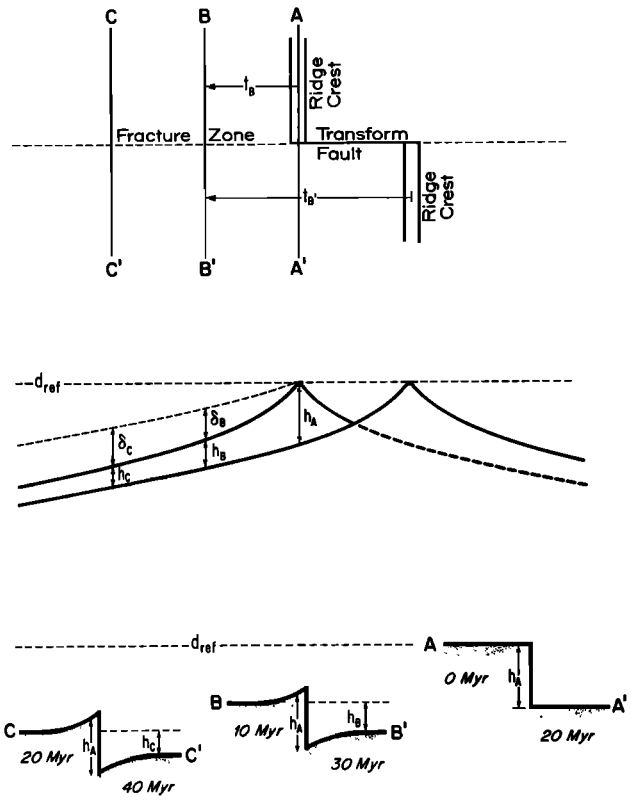

Fig. 1. Evolution of a fracture zone. (Top) Spreading ridges offset by a transform fault. The age offset across the FZ is $t_{B'} - t_B$. (Center) The h's are the differences in ocean floor depth between locations far to either side of the FZ. The initial height of the scarp at the FZ is h_A. If the FZ does not slip, the scarp height must remain constant. The constancy of scarp height and the decrease in h with age cause the lithosphere in the vicinity of the FZ to bend. The flexural amplitude δ_B is the difference between h_A and h_B. Similarly, $\delta_c = h_A - h_C$. (Bottom) Sketch of bathymetry along profiles A-A', B-B', and C-C' illustrating the lithospheric flexure described above.

and the vertical offset of distant ocean floor. Therefore the only adjustable model parameter is the stress relaxation temperature T_e which defines the base of the elastic layer. We will show that good fits between the observed and predicted bathymetric profiles are obtained by varying this single parameter. These good fits also confirm the absence of vertical slip on the fossil fault planes of the Mendocino and Pioneer FZ's.

The temperature dependence of h_e turns out to be an essential feature of the model; without it, flexure could not reproduce the curvature in the bathymetric profiles. Therefore this is independent evidence for the temperature dependence of h_e. The flexure models also yield estimates of the maximum bending stresses and average shear stresses in the lithosphere. We compare these with the magnitudes of the stresses caused by plate bending at ocean trenches. Finally, we calculate the flexure caused by horizontal conduction of heat across a FZ and demonstrate that it has a relatively small effect upon the bathymetry.

DATA

The Mendocino and Pioneer FZ's in the North Pacific were chosen to test our model of flexure at fracture zones primarily because they have a combined age offset of about 30 Myr and should therefore show large flexural amplitudes. The study region (Figure 2) was limited to the area between the Juan de Fuca ridge and 150°W because it contains identified magnetic anomalies [*Atwater and Menard,* 1970]. These anomalies were dated by using the magnetic time scale of *Ness et al.* [1980]. The Mendocino FZ has an age offset which varies between 30 Myr at 128°W and 25 Myr at 140°W. To the west of 140°W, the Mendocino divides and the age offset gradually shifts from the northern branch to the southern branch. However, only the total age offset across both FZ's is known, since the lithosphere between these two FZ's does not contain identified magnetic anomalies. The Pioneer FZ runs subparallel to the Mendocino FZ and has an age offset which varies between 8 Myr at its eastern end and 4 Myr at 104°W.

Five N-S trending bathymetric profiles crossing both FZ's were chosen for this study and are shown in Figure 2. A few other continuous N-S profiles are available; however, these additional profiles lie within 100 km of the five we have chosen, and they therefore contain redundant information. The depths along each of the profiles were obtained from the sounding charts used to construct the 'Bathymetry of the Northeast Pacific' contour map [*Mammerickx and Smith,* 1981]. The spacings between soundings varied from 1 to 2 min of latitude. Because of this rather coarse sampling the shortest wavelength topography is aliased, but the longer wavelength topographic features are unaffected.

The bathymetry along each of the profiles A–E in Figure 2 is shown in Figure 3 together with the ages of each lithospheric segment. The dashed lines are the bathymetric profiles predicted by the depth-age relation (equation (1) of the following section) and the parameter values in Table 1. The predicted depths are in approximate agreement with the data for locations more than 1° (111 km) away from each of the FZ's (marked by arrows in Figure 3). However, in the vicinity of each FZ there are large systematic differences between the predicted and observed depths. In each case, the ocean floor is anomalously shallow on the younger side of the FZ, while on the older side it is generally deeper than expected. We will show that the depth anomalies in Figure 3 are a consequence of lithospheric flexure.

MODEL

As the oceanic lithosphere ages, it cools and subsides according to the depth-age relation [*Parker and Oldenburg,*

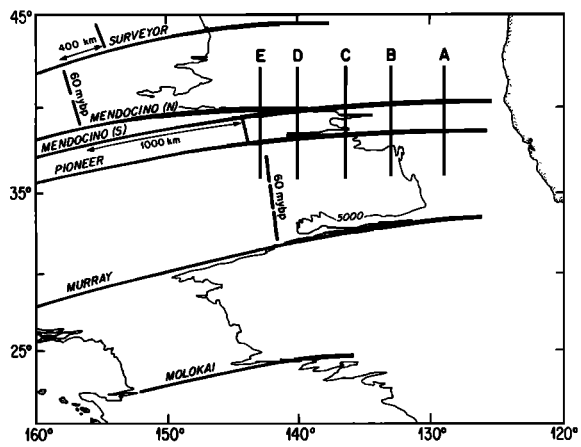

Fig. 2. Map of the northwest Pacific showing the locations of the five bathymetric profiles A–E crossing the Mendocino and Pioneer FZ's. The Mendocino FZ divides into north and south branches west of 140°W. Modified from *Mammerickx* [1982].

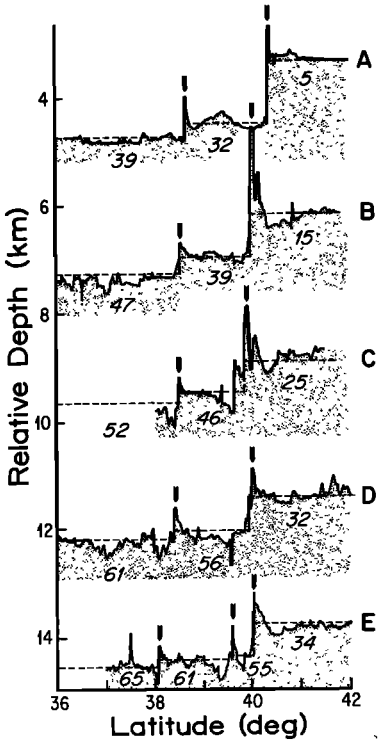

Fig. 3. Relative depth as a function of latitude along profiles A–E. Profiles are offset in increments of 2.3 km. Dashed lines are depths predicted from (1). FZ's are marked by arrows. The Pioneer FZ appears on each profile at 38°–39°N. The Mendocino FZ lies at ~40°N. The Mendocino S. is well defined on profile E at 39.6°N. It is seen that (1) predicts the overall change in depth across a FZ but not the scarp height.

1973; *Davis and Lister*, 1974; *Oxburgh and Turcotte*, 1978]

$$d(t) = d_{\text{ref}} + \frac{2\alpha\rho_m(T_m - T_s)}{(\rho_m - \rho_w)}\left(\frac{\kappa t}{\pi}\right)^{1/2} \quad (1)$$

for ages less than about 70 Myr [*Parsons and Sclater*, 1977].

The definitions of the parameters, and their values, are given in Table 1. Thus the bathymetric step h_A across the youngest part of the FZ, section A-A′ in Figure 1, is given by

$$h_A = d(t_{A'}) - d(0) = \frac{2\alpha\rho_m(T_m - T_s)}{(\rho_m - \rho_w)}\left(\frac{\kappa t_{A'}}{\pi}\right)^{1/2} \quad (2)$$

where $t_{A'}$ is the age offset across the FZ and $t_A = 0$. This bathymetric step is assumed to be frozen-in on the fossil fault plane as the FZ ages. However, the overall change in depth across the FZ decreases with age; along section B-B′ in Figure 1 it is h_B, where

$$h_B = d(t_{B'}) - d(t_B) = \frac{2\alpha\rho_m(T_m - T_s)}{(\rho_m - \rho_w)}\left(\frac{\kappa}{\pi}\right)^{1/2}(t_{B'}^{1/2} - t_B^{1/2}) \quad (3)$$

and t_B and $t_{B'}$ are the ages of the lithosphere at section B-B′. The amplitude of the flexure at B-B′ is

$$\delta_B = h_A - h_B = \frac{2\alpha\rho_m(T_m - T_s)}{(\rho_m - \rho_w)}\left(\frac{\kappa}{\pi}\right)^{1/2} \cdot \{(t_{B'} - t_B)^{1/2} + t_B^{1/2} - t_{B'}^{1/2}\} \quad (4)$$

where $t_{A'} = t_{B'} - t_B$. A contour plot of this flexural amplitude is shown in Figure 4 in terms of the age of the younger side of the FZ and the age offset. While flexural amplitude increases continuously with age, the rate of increase declines with age, and most of the amplitude is acquired while the FZ is young.

The wavelength of the flexure λ is given by

$$\lambda = 2\pi\left(\frac{4D}{g(\rho_m - \rho_w)}\right)^{1/4} \quad (5)$$

where D, the flexural rigidity, is

$$D = \frac{Eh_e^3}{12(1 - \nu^2)} \quad (6)$$

TABLE 1. Definitions and Values of Parameters and Functions

Parameter	Definition	Value	Reference
α	thermal expansion coefficient	3.1×10^{-5} K^{-1}	*Parsons and Sclater* [1977]
d_{ref}	ridge crest depth	2500 m	*Parsons and Sclater* [1977]
E	Young's modulus	6.5×10^4 MPa	
g	acceleration of gravity	9.82 m s^{-2}	
κ	thermal diffusivity	8×10^{-7} m^2 s^{-1}	*Parsons and Sclater* [1977]
ν	Poisson's ratio	0.25	
ρ_m	mantle density	3330 kg m^{-3}	
ρ_w	seawater density	1025 kg m^{-3}	
T_e	stress relaxation temperature	450°C	*Watts et al.* [1980]
T_m	mantle temperature	1365°C	*Parsons and Sclater* [1977]
T_s	surface temperature	0°C	

Function	Definition	Units
d	ocean floor depth	meters
δ	flexural amplitude	meters
D	flexural rigidity	newton-meters
h	overall change in depth across a fracture zone	meters
h_e	effective elastic thickness	meters
λ	flexural wavelength	meters
σ_{xx}	bending stress	megapascals
σ_{xz}	shear stress	megapascals
w	flexural topography	meters

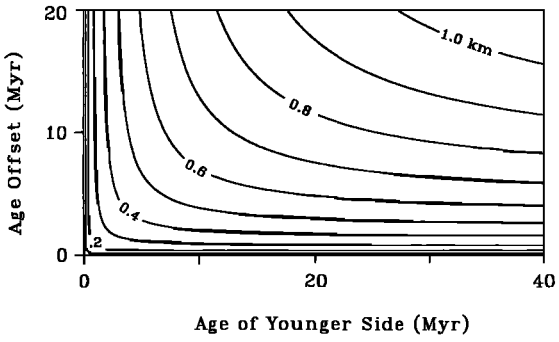

Fig. 4. Contours of flexural amplitude δ (calculated from (4)) as a function of the age offset across the FZ and the age on the younger side of the FZ. At constant age offset, δ increases most rapidly at young ages. Small age offset FZ's (e.g., 1 Myr) have flexural amplitudes of several hundred meters.

The effective elastic thickness h_e is related to age t by [*Caldwell and Turcotte*, 1979]

$$h_e = 2(\kappa t)^{1/2}\,\mathrm{erfc}^{-1}\left(\frac{T_m - T_e}{T_m - T_s}\right) \tag{7}$$

where erfc^{-1} is the inverse complimentary error function. Upon combining (5)–(7) we obtain

$$D = \frac{2E(\kappa t)^{3/2}}{3(1-\nu^2)}\left\{\mathrm{erfc}^{-1}\left(\frac{T_m - T_e}{T_m - T_s}\right)\right\}^3 \tag{8}$$

and

$$\lambda = 2\pi\left(\frac{8E}{3g(\rho_m - \rho_w)(1-\nu^2)}\right)^{1/4} \cdot (\kappa t)^{3/8}\left\{\mathrm{erfc}^{-1}\left(\frac{T_m - T_e}{T_m - T_s}\right)\right\}^{3/4} \tag{9}$$

The lithosphere on the younger side of the FZ flexes with a shorter wavelength than the lithosphere on the older side of the FZ because $\lambda \propto t^{3/8}$. In addition, the flexural wavelength on either side of the FZ increases as the FZ ages.

In calculating the flexural topography as a function of age along a FZ we have approximated the continuous time dependences of δ and λ by using discrete 1 Myr time steps. Because the flexural problem is linear, the total flexural topography is the sum of the incremental contributions over all of the steps up to the age of the FZ.

The separation distance between the Pioneer and Mendocino FZ's (150–220 km) is less than one flexural wavelength when the age of the lithosphere between the two FZ's is greater than about 10 Myr. This produces a coupling of the FZ's and requires that the flexural problem be formulated so as to explicitly include the interaction. We have actually modelled the most general case in which $N + 1$ segments of lithosphere are separated by N FZ's. This configuration of FZ's is shown in Figure 5 for the case $N = 2$. The ith segment of lithosphere has a flexural rigidity D_i that depends upon its age t_i according to (8). The ith FZ is located at x_i and the flexural topography between the ith and $(i + 1)$th FZ's is $w_{i+1}(x)$. The flexural amplitude at the ith FZ is δ_i; it is a function of the ages of the adjacent lithospheric segments and the duration of the time step since the previous increment of flexure.

The $N + 1$ homogeneous differential equations governing the flexural topography are

$$D_1\frac{d^4w_1}{dx^4} + g(\rho_m - \rho_w)w_1 = 0 \qquad x < x_1$$

$$D_i\frac{d^4w_i}{dx^4} + g(\rho_m - \rho_w)w_i = 0 \qquad x_{i-1} < x < x_i \tag{10}$$

$$D_{N+1}\frac{d^4w_{N+1}}{dx^4} + g(\rho_m - \rho_w)w_{N+1} = 0 \qquad x_N < x$$

Their solutions are

$$w_i(x) = e^{-2\pi x/\lambda_i}\left\{A_i \sin\frac{2\pi x}{\lambda_i} + B_i\cos\frac{2\pi x}{\lambda_i}\right\} + e^{2\pi x/\lambda_i}\left\{C_i\sin\frac{2\pi x}{\lambda_i} + D_i\cos\frac{2\pi x}{\lambda_i}\right\} \tag{11}$$

for $x_{i-1} < x < x_i$, where λ_i is given by (9) with $t = t_i$. The coefficients A_i, B_i, C_i, and D_i are determined from the boundary conditions and matching conditions discussed below.

For $N + 1$ lithospheric segments there are $4(N + 1)$ coefficients to be determined. The boundary conditions require that the flexural topography must vanish as $x \to \pm\infty$. This condition is satisfied if the four coefficients A_1, B_1, C_{N+1}, D_{N+1} are zero. The remaining $4N$ coefficients are determined from four matching conditions at each of the N FZ's. At the ith FZ the displacement must be discontinuous by the amount δ_i, while the slope, moment, and shear force must all be continuous. The matching conditions at $x = x_i$ are therefore

$$w_i - w_{i+1} = \delta_i \tag{12}$$

$$\frac{dw_i}{dx} - \frac{dw_{i+1}}{dx} = 0 \tag{13}$$

$$-D_i\frac{d^2w_i}{dx^2} + D_{i+1}\frac{d^2w_{i+1}}{dx^2} = 0 \tag{14}$$

$$-D_i\frac{d^3w_i}{dx^3} + D_{i+1}\frac{d^3w_{i+1}}{dx^3} = 0 \tag{15}$$

We have solved these $4N$ equations by a method similar to the Thompson-Haskell technique [*Haskell*, 1953] used to determine the eigenfunctions and eigenfrequencies for Rayleigh and Love waves in a layered half space.

Once the coefficients have been determined, the flexural

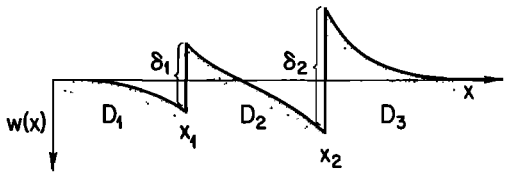

Fig. 5. Model used to calculate the flexural topography $w(x)$ across multiple FZ's. Two FZ's are located at x_1 and x_2 and have flexural amplitudes δ_1 and δ_2. The flexural rigidity is different for each segment of lithosphere.

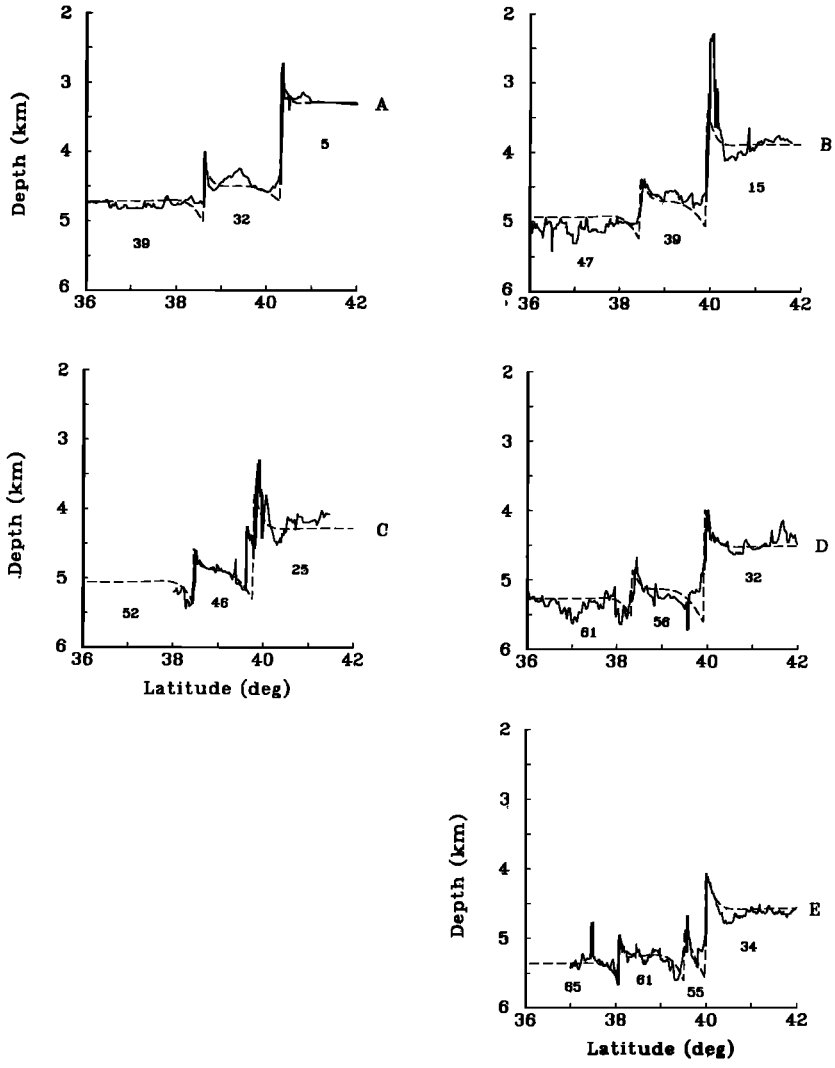

Fig. 6. Comparisons between theoretical bathymetric profiles computed from flexure models assuming no slip on the FZ's (dashed lines) and the observed bathymetric profiles A–E (solid lines). The asymmetric flexure predicted by the model across each FZ is a consequence of the increase in flexural wavelength with age according to (9). The apparent tilt in the bathymetry between the Pioneer and Mendocino FZ's occurs because the flexural wavelength is greater than their separation distance.

topography can be calculated from (11). Other quantities of interest are the maximum bending stresses σ_{xx} and the average shear stresses σ_{xz} in the elastic lithosphere. The maximum bending stress at the top of the ith lithospheric segment is

$$\sigma_{xx_i}(x) = \frac{-Eh_e}{2(1-\nu^2)} \frac{d^2w_i}{dx^2}(x) = \frac{6M_i(x)}{h_e^2} \tag{16}$$

where $M_i(x)$ is the bending moment

$$M_i(x) = -D_i \frac{d^2w_i}{dx^2}(x) \tag{17}$$

The average shear stress σ_{xz} is the shear force divided by h_e

$$\sigma_{xz_i}(x) = \frac{-D_i}{h_e} \frac{d^3w_i}{dx^3}(x) \tag{18}$$

The total bathymetry across a FZ is found by calculating the flexural topography for each time step from zero to the age of the FZ, summing the flexure over all of the time steps, and finally adding this flexural topography along each lithospheric segment to the depths calculated from the depth-age relation.

RESULTS

Figure 6 shows comparisons between model depths (dashed lines) and the five bathymetric profiles (solid lines). The values of the thermal parameters α, κ, and T_m used in these model calculations are compatible with the depth-age and heat flow–age relations from the North Pacific [*Parsons and Sclater*, 1977]. The value of the stress relaxation temperature T_e was adjusted until good fits were obtained for all five profiles. The models shown in Figure 6 were calculated using $T_e = 450$°C although reasonable fits were also obtained for values of T_e ranging from 350°C to 600°C.

The model predicts many of the features that appear in the observed profiles. In nearly every case the observed flexural amplitude is well matched by the model. This agreement

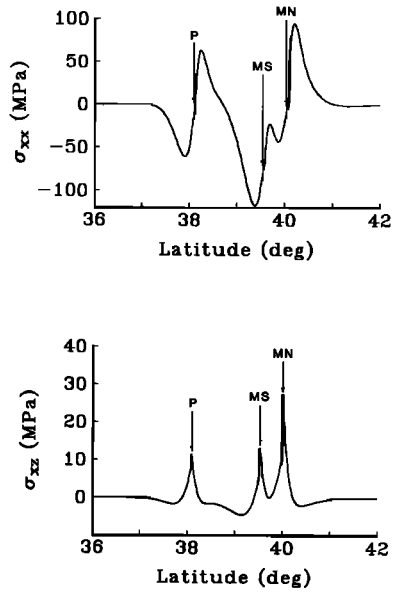

Fig. 7. Stresses along profile E. (Top) Maximum bending stress σ_{xx} at the top of the elastic layer. Arrows indicate locations of FZ's (P—Pioneer; MS—Mendocino S.; MN—Mendocino N.). (Bottom) Average shear stress σ_{xz} within the elastic layer. Peaks occur at the three FZ's.

indicates that these FZ's have not slipped significantly during their evolutions. The largest differences between the model and the data occur on the young side of the Mendocino FZ along profiles B and C. Equation (4) predicts only about one half of the Mendocino scarp amplitude along profile B. The excess scarp amplitude may have been produced when the velocity vector of the Pacific plate was not parallel to the now subducted Mendocino transform fault [*Menard and Atwater*, 1969].

The asymmetry of the flexure about each FZ is a consequence of the increase in effective elastic thickness with age. This asymmetry is most apparent on profiles B–E, where the flexural wavelength on the young side of each FZ is shorter than the flexural wavelength on the older side. Initially, we modelled the flexure on these FZ's with a constant h_e. However, these models failed to fit the observed profiles, since they could not reproduce the asymmetric flexure pattern. Thus the flexure at these FZ's is independent evidence that h_e increases with age.

Probably the most pronounced flexural feature that appears on profiles B–E is the tilting (downward to the north) of the segment of lithosphere that lies between the Mendocino and Pioneer FZ's. This tilting occurs because the separation distance between the two FZ's is less than the flexural wavelength at the age when much of the flexure occurred. Thus stresses are transmitted between the two FZ's, and it is necessary to solve for the flexural topography across both FZ's simultaneously.

Considering the good overall agreement between the observed bathymetry and the ocean floor depths predicted by the model, we believe that the characteristic ridge and trough topographic pattern at the Mendocino and Pioneer FZ's is the flexural response of the lithosphere to the differences in subsidence rates across the FZ's and the absence of slip on the FZ's. No significant vertical slip has taken place during the evolutions of these FZ's in spite of the large flexural amplitudes (about 1 km) that must be sustained by stresses transmitted across the fossil transform faults for periods of greater than 50 Myr.

The maximum bending stress σ_{xx} (measured at the top of the elastic layer) and the average shear stress σ_{xz} along each profile have been calculated from the flexure model by summing (16) and (18) over the time increments. The largest stresses occur along profile E, and these are shown in Figure 7. The locations of the three FZ's are also marked in this figure. Relative minima and maxima of σ_{xx} occur at points lying about 10–20 km to the south and north of each FZ, respectively. The largest maximum bending stress of −120 MPa occurs just south of the Mendocino S. FZ. The largest average shear stress of 28 MPa is found at the Mendocino N. FZ. The maximum values of $|\sigma_{xx}|$ and $|\sigma_{xz}|$ attained along the other profiles are summarized in Table 2.

To test whether lithospheric flexure occurs at other major Pacific FZ's, we have modelled bathymetric profiles crossing the Clipperton, Clarion, Molokai, and Murray FZ's. The most complete N-S bathymetric coverage in the North Pacific occurs at 140°W where a number of cruises span the latitudes between 4°N and 41°N [*Mammerickx and Smith*, 1981]. The locations of two of these ship tracks are shown in Figure 8*a* (dashed lines) together with the locations of the major FZ's (solid lines). The modelling of these bathymetric profiles requires that the age of each lithospheric segment be known. North of the Molokai FZ ages were determined from identified magnetic anomalies. South of the Molokai FZ there are no identified anomalies. However, along 140°W there are a number of deep-sea drilling sites which can be used to constrain basement ages. Site 162, which lies just to the south of the Clarion FZ, reached basement with an age of 49.5 ± 3.6 Myr [*Van Andel and Bukry*, 1973]. Other sites which did not reach basement were used to place minimum bounds upon ages and sediment thicknesses. For example, sites 70 and 71 lie just to the north and south of the Clipperton FZ, respectively, and have minimum age/sediment thickness of 46 Myr/338 m and 37 Myr/558 m, respectively. Where ages are uncertain (annotated by question marks in Figure 8*b*), we chose the age that would match the average seafloor depth away from the FZ based on the depth-age relation of *Parsons and Sclater* [1977]. At the Clipperton FZ, however, sediment thickness exceeds 300 m. Along this profile, ages were based upon seafloor depths corrected for sediment loading.

Figure 8*b* shows a comparison of the flexure model profiles (dashed lines) with each of the observed bathymetric profiles (solid lines). Except for the Clipperton FZ and the south side of the Murray FZ, the flexure model is compatible

TABLE 2. Maximum Stresses (Megapascals)

	Mendocino N.		Mendocino S.		Pioneer	
Profile	$\lvert\sigma_{xx}\rvert$	$\lvert\sigma_{xz}\rvert$	$\lvert\sigma_{xx}\rvert$	$\lvert\sigma_{xz}\rvert$	$\lvert\sigma_{xx}\rvert$	$\lvert\sigma_{xz}\rvert$
A	70	20	...	...	72	13
B	88	28	...	...	76	18
C	92	29	...	...	67	16
D	98	30	...	...	68	14
E	95	28	122	14	60	13

In every case the maximum shear stress $|\sigma_{xz}|$ occurs at the FZ. The maximum of $|\sigma_{xx}|$ occurs 10–20 km north of each FZ except for the Mendocino S. on profile E where it occurs 20 km south of the FZ.

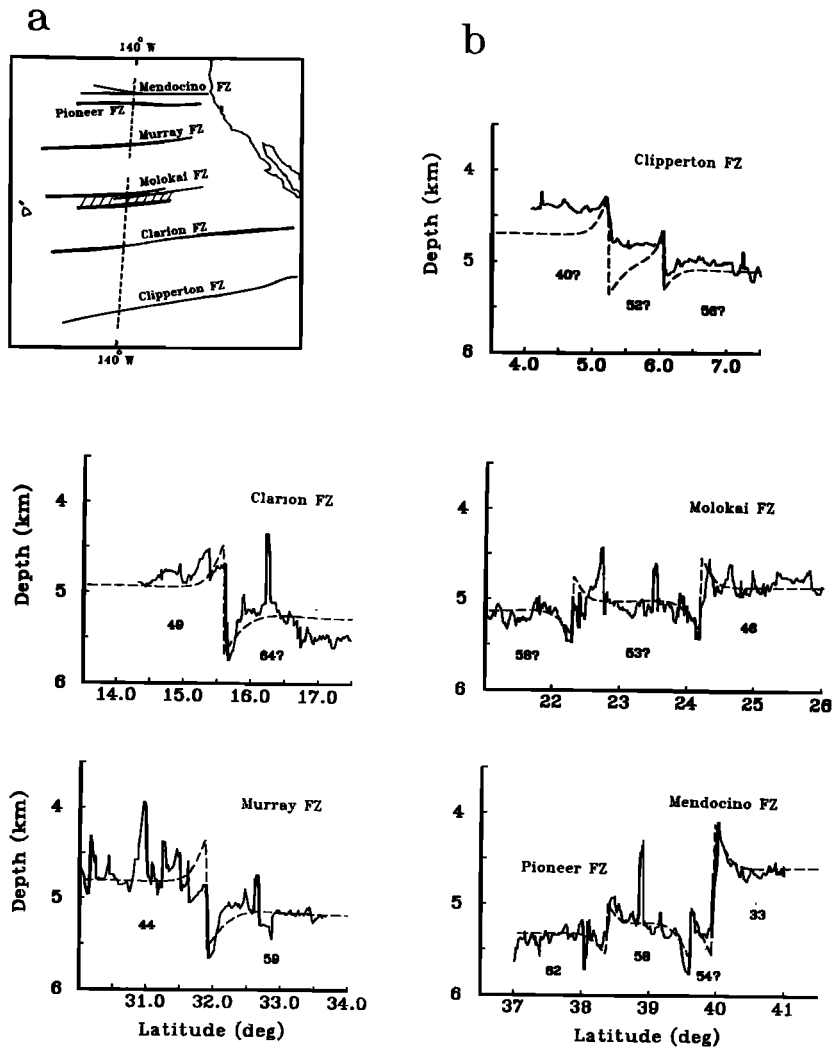

Fig. 8. (*a*) Location map (gnomonic projection) of major North Pacific fracture zones. Dashed lines indicate ship tracks. (*b*) Comparison of flexure model (dashed curve) with bathymetry across each of the major FZ's. Question marks indicate that ages are based upon the depth-age relation.

with the observations. From these comparisons alone, however, one cannot determine if any slip has occurred on the fracture zones. The important result is that the observations do not disagree with the flexural model for the Clipperton, Clarion, Molokai, and Murray FZ's and the agreement between the model and the data is again quite good across the Mendocino FZ where the age offset is greatest.

Effects of Horizontal Heat Conduction

In this section we demonstrate that horizontal conduction of heat across the FZ has only a minor influence upon the bathymetry and that it is valid to neglect this effect in computing the model bathymetric profiles of Figure 6. In writing the depth-age relation (1) we assumed that the thermal structure of the FZ is given by the half-space cooling model

$$T(z, t) = (T_m - T_s)\,\mathrm{erf}\left(\frac{z}{2(\kappa t)^{1/2}}\right) + T_s \qquad (19)$$

where z is the depth beneath the ocean floor and t is the age of the half space. This gives a step change in temperature across the FZ as a consequence of the age offset. Actually, the temperature will vary in a continuous manner across the FZ because of horizontal heat conduction [*Louden and Forsyth*, 1976]. The deviations in temperature from the step variation implied by (19) are responsible for buoyancy forces on the lithosphere which flex the younger lithosphere down and the older lithosphere up. The sense of this additional flexure is opposite to that of the flexure caused by the difference in subsidence rates. (The two effects were separated to avoid a numerical solution to the complete problem.)

The two-dimensional temperature structure along B-B′ in Figure 1 is derived in Appendix A;

$$T(x, z) = T_s + \frac{(T_m - T_s)}{2}\left\{\mathrm{erfc}\left(\frac{x}{2(\kappa t_B)^{1/2}}\right)\mathrm{erf}\left(\frac{z}{2(\kappa t_B)^{1/2}}\right) + \mathrm{erfc}\left(\frac{-x}{2(\kappa t_B)^{1/2}}\right)\mathrm{erf}\left(\frac{z}{2(\kappa t_{B'})^{1/2}}\right)\right\} \qquad (20)$$

The temperature due solely to horizontal heat conduction $\Delta T(x, z)$ is found by constructing the step variation from (19)

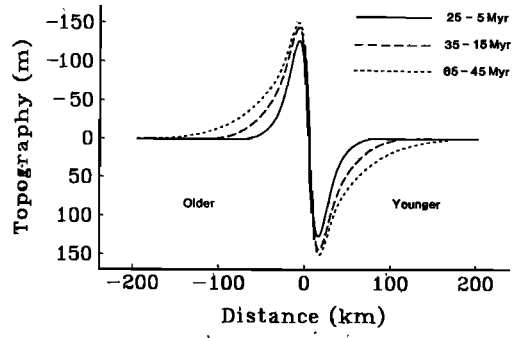

Fig. 9. Flexural topography associated with heat conduction across a FZ with a 20-Myr age offset. Ages of younger side are 5 Myr (solid line), 15 Myr (dashed line), and 45 Myr (dotted line). This topography broadens with age as heat diffuses across the FZ. The amplitude of this effect has been overestimated, especially on the older side of the FZ, since we used the flexural rigidity-age relation (8) of the younger side of the FZ in the theoretical calculation.

and subtracting it from (20):

$$\Delta T(x, z) = \frac{(T_m - T_s)}{2}\left\{\left(\operatorname{erfc}\left(\frac{-x}{2(\kappa t_B)^{1/2}}\right) - 2H(x)\right]\cdot\left[\operatorname{erf}\left(\frac{z}{2(\kappa t_{B'})^{1/2}}\right) - \operatorname{erf}\left(\frac{z}{2(\kappa t_B)^{1/2}}\right)\right]\right\} \quad (21)$$

where $H(x)$ is the Heaviside step function. The buoyancy forces arising from these temperature differences exert a pressure on the base of the lithosphere $p(x)$ given by

$$p(x) = -g\alpha\rho_m \int_0^\infty \Delta T(x, z)\, dz \quad (22)$$

where α is the coefficient of thermal expansion. Upon substituting (21) into (22) and performing the integration we find

$$p(x) = -g\alpha\rho_m(T_m - T_s)\left(\frac{\kappa}{\pi}\right)^{1/2}((t_{B'})^{1/2} - (t_B)^{1/2})\left\{2H(x) - \operatorname{erfc}\left(\frac{-x}{2(\kappa t_B)^{1/2}}\right)\right\} \quad (23)$$

The pressure force is measured positive downward to be consistent with our sign convention for the flexural topography w.

The deflection of the lithosphere produced by this pressure is found by solving the equation for the thin elastic plate model [*Turcotte*, 1979]:

$$D\frac{d^4w}{dx^4} + g(\rho_m - \rho_w)w = p(x) \quad (24)$$

subject to the conditions that w and dw/dx approach zero as x tends to $\pm\infty$. To avoid the necessity of resorting to a numerical solution of (24), we will assume that D is constant across the FZ and has the value appropriate to the age of the lithosphere on the younger side of the FZ according to (8). This is a conservative assumption for the value of D, since it actually overestimates the flexural topography caused by lateral heat conduction.

Equation (24) is most easily solved by taking its Fourier transform [*Banks et al.*, 1977]. We obtain

$$W(k) = \left(1 + \frac{D|k|^4}{g(\rho_m - \rho_w)}\right)^{-1}\frac{2\alpha\rho_m(T_m - T_s)}{(\rho_m - \rho_w)}\left(\frac{\kappa}{\pi}\right)^{1/2}\cdot[(t_{B'})^{1/2} - (t_B)^{1/2}]\cdot\frac{i}{k}[1 - \exp(-k^2\kappa t_B)] \quad (25)$$

where k is the wave number and $W(k)$ is the Fourier transform of $w(x)$. To obtain the topography $w(x)$, we invert (25) numerically using a fast Fourier transform procedure. The age dependence of $D = D(t_B)$ is accounted for by applying (25) to discrete 1-Myr time intervals using the value of D appropriate to the interval and incrementing the plate deflection throughout the evolution of the FZ.

Figure 9 shows the topography due to horizontal heat conduction across a FZ with a 20-Myr age offset when the age of the younger side of the FZ is 5, 15, and 45 Myr. The magnitude of this flexural topography increases with the age of the FZ. The effects of horizontal heat conduction on the topography extend progressively farther from the FZ as it ages. The flexural amplitude does not decrease as the thermal contrast (21) across the FZ decreases with age because each increment of flexural topography becomes frozen in as the elastic lithosphere thickens from below. We have seen in the model section that the flexural wavelength increases with age proportionately to $t^{3/8}$, while the thermal diffusion distance increases as $t^{1/2}$. Horizontal heat conduction does not change the flexural amplitude given by (4); it tends only to broaden the topographic profile. This is because the scarp height on the FZ is frozen in and the differential subsidence far from the FZ is unaffected by heat conduction across the FZ. In agreement with this, the topography in Figure 9 is zero both at $x = 0$ and $x = \pm\infty$.

The amplitude of the topography in Figure 9 is about 150 m. This is to be compared with the observed flexural amplitude of 500 m on profiles B–E in Figure 6. It should be remembered that the topography of Figure 9 significantly overestimates the effect of horizontal heat conduction on the older side of the FZ and may slightly overestimate it on the younger side because of our approximation to D. Therefore while flexure due to horizontal heat conduction is small, it is not entirely negligible. In fact it may be responsible for the dips in the bathymetric profiles B–E on the north side of the Mendocino FZ (Figure 6).

Discussion and Conclusions

Global, regional, and local seismicity studies indicate that FZ's do not slip over periods of time short enough to generate seismic disturbances. The majority of earthquakes with magnitudes greater than about 5 occur along plate boundaries including subduction zones, spreading centers, and transform faults [*Barazangi and Dorman*, 1969]. Large intraplate earthquakes rarely occur. A regional study of smaller intraplate earthquakes (magnitude greater than about 4) in the south central Pacific showed that only one earthquake out of about 100 occurred at a FZ [*Okal et al.*, 1980]. Local studies of microseismicity at the intersections of transform faults, spreading ridges, and fracture zones demonstrate that while numerous microearthquakes occur along the transform faults and spreading ridges, the FZ's are seismically inactive [*Reid*, 1976; *Francis et al.*, 1978; *Forsyth and Rowlett*, 1979; *Rowlett*, 1981].

Our study indicates that at least two major FZ's do not slip

over a time scale of 10^7 yr, ruling out the possibility of aseismic slip on the FZ's. The models of the flexural topography across profiles A–E (Figure 6) predict that the fossil transform faults must maintain shear stresses of up to 30 MPa. These stresses are more than twice as large as the stress drops derived from studies of major earthquakes [*Brune*, 1968]. If a FZ were a zone of weakness, then it should slip, like other faults, to relieve these large shear stresses. We conclude, therefore, that a FZ is not a zone of weakness; the fractured crust is only a remnant surface expression of past tectonic activity along the transform fault and spreading ridges. Beneath this fractured surface layer lies coherent oceanic lithosphere that is not significantly weaker than the surrounding lithosphere. This is not surprising when one considers the evolution of a FZ. The lithosphere on the younger side of the FZ is created by upwelling of hot mantle material along the ridge crest which terminates at the end of the transform fault (see Figure 1). The material upwelling at this intersection cools rapidly because of its proximity to the older segment of lithosphere. Thus the two segments of lithosphere fuse together at this intersection. The mechanical bond continues to increase in strength as the FZ ages. At depth, the FZ is not a structural boundary; instead it is a zone of large horizontal temperature gradients.

Our observation that the Pioneer and Mendociono FZ's have not slipped significantly during their evolutions has implications for FZ's with much smaller age offsets and for FZ's situated on very old lithosphere. In both cases, the ridge and trough features predicted by our model should have sufficient amplitude to appear on large-scale bathymetric charts with 100- or 200-m contour intervals.

Consider the older portions of the Mendocino FZ separating lithospheric segments of ages 135 Myr and 140 Myr [*Mammerickx*, 1982]. The overall change in depth across this FZ is only 30 m according to the empirical depth-age relation of *Parsons and Sclater* [1977]. If this were the only topographic expression of the FZ, then it would not be apparent on a bathymetric chart with a 100-m contour interval. However, the FZ is clearly delineated on the map of this region. Furthermore, the step in the bathymetry across a 500-km segment of this FZ lying between the Hawaiian-Emperor ridge and the Mapmaker Seamounts varies from 300 to 700 m (see Figure 3 of *Mammerickx* [1982]). Our model predicts a step amplitude of 715 m along this portion of the Mendocino FZ. The agreement, although not perfect, indicates that this portion of the Mendocino FZ has not slipped significantly for over 130 Myr.

FZ's with very small age offsets should also be visible on bathymetric charts with a 100-m contour interval even when the overall change in ocean floor depth far from the FZ is less than 100 m. For example, (4) predicts that the bathymetric step across a FZ separating lithospheric segments with ages of 30 and 31 Myr is more than 300 m (see Figure 2). The overall change in ocean floor depth far from the FZ is only 32 m in this case.

Fracture zones with both large and small age offsets can be traced for thousands of kilometers across the ocean floor. If FZ's slipped completely during their evolutions, then their topographic expressions would diminish with age. However, the FZ topography persists on lithosphere with ages greater than 100 Myr. Some of this topography may be the result of fracturing in the transform fault environment. However, the major topographic expression of Pacific FZ's (i.e., the ridge and trough) is a consequence of the freezing in of the bathymetric step at the intersection of the transform fault with the ridge crest.

From an examination of Atlantic bathymetric charts it is evident that the ridges and troughs that are characteristic of Pacific FZ's are not the dominant topographic expression of Atlantic FZ's. Atlantic FZ's generally consist of a narrow deep central valley surrounded by bordering ridges [*Van Andel et al.*, 1971]. Our flexural model cannot explain this type of topography which apparently forms within the active transform fault environment. Furthermore, the amplitude of the topography along large age offset Atlantic FZ's is generally 1–3 km (see Figure 4 of *Feden et al.* [1975]). This is greater than the expected flexural amplitude (<1 km), and therefore it may mask any flexure that has occurred along Atlantic FZ's. Detection of flexural topography associated with Atlantic FZ's is also made difficult by the roughness of the seafloor. The seafloor of the Atlantic is generally rougher than Pacific seafloor perhaps because of the difference in spreading rates [*Menard*, 1967]. As a consequence of the general roughness of the Atlantic seafloor and the large valleys and hills that are formed within Atlantic transform faults it may be impossible to observe any flexure along Atlantic FZ's.

Lithospheric flexure at the Mendocino and Pioneer FZ's is qualitatively similar to the bending of the lithosphere at subduction zones and around large seamounts. The main difference is that the maximum bending stresses inferred from subduction zone and seamount studies are usually greater than 500 MPa, while the stresses at FZ's are substantially lower, about 100 MPa. Experimental and theoretical studies of lithospheric rheology indicate that the largest stresses inferred from purely elastic subduction zone models ($\sim 10^3$ MPa) cannot be maintained [*Kirby*, 1980]. Accordingly, flexure at subduction zones has been reinterpreted with more realistic elastic-plastic rheologies [*Turcotte et al.*, 1978; *McAdoo et al.*, 1978; *Chapple and Forsyth*, 1979; *Forsyth*, 1980; M. K. McNutt and H. W. Menard, unpublished manuscript, 1981]. In these models, the lithosphere behaves elastically until the yield stress is reached, at which point further increases in strain do not increase the stress (plastic behavior). Yield stress depends on temperature, overburden pressure, strain rate, and the sign of the stress (i.e., tension or compression). In contrast to the situation at subduction zones, the maximum bending stresses at FZ's are probably smaller than the yield stresses and purely elastic models of the bending should suffice. The most important rheological consideration for modelling of lithospheric flexure at FZ's is the increase of effective elastic thickness with age. Our attempts to match the observed flexural topography at FZ's with a constant h_e were not successful.

Our major conclusions are as follows:

1. There is no significant slip on the fossil fault planes of the Mendocino and Pioneer FZ's. The bathymetric steps on these FZ's are constant with age and equal to the initial vertical offsets at the ridge–transform fault–FZ intersections.

2. As a consequence of the frozen-in scarp and the differential subsidence of lithosphere far from the FZ, the lithosphere bends in the vicinity of the FZ. This flexure results in a characteristic ridge-trough topographic signature. The flexural amplitude, which is the difference between the scarp height and the overall change in depth across the FZ, increases with age.

3. Good fits to the bathymetric profiles across the Mendocino and Pioneer FZ's can be obtained by modelling the

topography as the flexure of a thin elastic plate with an age-dependent effective elastic thickness.

4. Results of the modelling indicate that the base of the elastic lithosphere is approximately defined by the 450°C isotherm. Maximum bending stresses are on the order of 100 MPa, substantially less than the stresses encountered at subduction zones.

5. Because the separation of the Mendocino and Pioneer FZ's is less than a flexural wavelength, there is elastic coupling between them.

APPENDIX: TEMPERATURES IN THE VICINITY OF A FRACTURE ZONE

The two-dimensional thermal structure near a FZ is found by solving the time-dependent heat conduction equation

$$\frac{\partial^2 T}{\partial x^2} + \frac{\partial^2 T}{\partial z^2} = \frac{1}{\kappa}\frac{\partial T}{\partial t} \tag{A1}$$

where z is depth and x is distance from the fossil transform fault. The initial temperature distribution $T(x, z, t_{A'})$ is that appropriate to the lithosphere lying beneath A-A' in Figure 1 [*Louden and Forsyth*, 1976]

$$\begin{aligned} T(x, z, t_{A'}) &= T_m & x < 0 \\ T(x, z, t_{A'}) &= T_s + (T_m - T_s)\,\mathrm{erf}\left(\frac{z}{2(\kappa t_{A'})^{1/2}}\right) & x > 0 \end{aligned} \tag{A2}$$

The boundary condition is

$$T(x, 0, t) = T_s \tag{A3}$$

The solution to this problem for an arbitrary initial temperature distribution can be expressed as a two-dimensional convolution of the initial temperature with a line source Green's function

$$T'(x, z, t) = \int_0^\infty \int_{-\infty}^\infty \cdot\, T'(x_0, z_0, t_{A'}) G(x - x_0, z - z_0, t - t_{A'})\, dx_0\, dz_0 \tag{A4}$$

where $T' \equiv T - T_s$ and the Green's function is [*Carslaw and Jaeger*, 1959]

$$\begin{aligned} G(x - x_0, z - z_0, t - t_{A'}) = {} & \frac{1}{4\pi\kappa(t - t_{A'})} \\ & \cdot \{\exp[-((x - x_0)^2 + (z - z_0)^2)/4\kappa(t - t_{A'})] \\ & - \exp[-((x - x_0)^2 + (z + z_0)^2)/4\kappa(t - t_{A'})]\} \end{aligned} \tag{A5}$$

After inserting (A2) into (A4) and integrating over x_0 and z_0 we find

$$\begin{aligned} T'(x, z, t) = {} & \frac{(T_m - T_s)}{2} \\ & \cdot \left[\mathrm{erfc}\left(\frac{x}{2[\kappa(t - t_{A'})]^{1/2}}\right)\mathrm{erf}\left(\frac{z}{2[\kappa(t - t_{A'})]^{1/2}}\right)\right. \\ & \left. + \mathrm{erfc}\left(\frac{-x}{2[\kappa(t - t_{A'})]^{1/2}}\right)\mathrm{erf}\left(\frac{z}{2(\kappa t)^{1/2}}\right)\right] \end{aligned} \tag{A6}$$

where $t - t_{A'}$ is the age of the lithosphere on the younger side of the FZ and t is the age on the older side. The actual temperature is obtained by adding T_s to T'.

Acknowledgments. We thank Jacqueline Mammerickx for providing the bathymetric data. This research was supported by the NASA Geodynamics program under grant NAG 5152.

REFERENCES

Atwater, T., and H. W. Menard, Magnetic lineations in the northeast Pacific, *Earth Planet. Sci. Lett.*, *7*, 445–450, 1970.

Banks, R. J., R. L. Parker, and J. P. Huestis, Isostatic compensation on a continental scale: Local versus regional mechanisms, *Geophys. J. R. Astron. Soc.*, *51*, 431–452, 1977.

Barazangi, M., and J. Dorman, World seismicity map of ESSA Coast and Geodetic Survey epicenter data for 1961–1967, *Bull. Seismol. Soc. Am.*, *59*, 369–376, 1969.

Bodine, J. H., M. S. Steckler, and A. B. Watts, Observations of flexure and the rheology of the oceanic lithosphere, *J. Geophys. Res.*, *86*, 3695–3707, 1981.

Brune, J. M., Seismic moment, seismicity, and rate of slip along major fault zones, *J. Geophys. Res.*, *73*, 777–785, 1968.

Caldwell, J. G., and D. L. Turcotte, Dependence of the thickness of the elastic oceanic lithosphere on age, *J. Geophys. Res.*, *84*, 7572–7576, 1979.

Caldwell, J. G., W. F. Haxby, D. E. Karig, and D. L. Turcotte, On the applicability of a universal elastic trench profile, *Earth Planet. Sci. Lett.*, *31*, 239–246, 1976.

Carslaw, H. S., and J. C. Jaeger, *Conduction of Heat in Solids*, 510 pp., Oxford University Press, New York, 1959.

Chapple, W. M., and D. W. Forsyth, Earthquakes and bending of plates at trenches, *J. Geophys. Res.*, *84*, 6729–6749, 1979.

Davis, E. E., and C. R. B. Lister, Fundamentals of ridgecrest topography, *Earth Planet. Sci. Lett.*, *21*, 405–413, 1974.

DeLong, S. E., J. F. Dewey, and P. J. Fox, Displacement history of oceanic fracture zones, *Geology*, *5*, 199–202, 1977.

Feden, R. H., H. S. Fleming, R. K. Perry, and J. D. Phillips, The mid-Atlantic ridge at 33°N: The Hayes fracture zone, *Earth Planet. Sci. Lett.*, *26*, 292–298, 1975.

Forsyth, D. W., Comparison of mechanical models of the oceanic lithosphere, *J. Geophys. Res.*, *85*, 6364–6368, 1980.

Forsyth, D., and H. Rowlett, Microearthquakes and recent faulting at the intersection of the Vema Fracture Zone and the Mid-Atlantic Ridge (abstract), *Eos Trans. AGU*, *60*, 376, 1979.

Francis, T. J. G., I. T. Porter, and R. C. Lilwall, Microearthquakes near the eastern end of the St. Paul's Fracture Zone, *Geophys. J. R. Astron. Soc.*, *53*, 201–217, 1978.

Gunn, R., A quantitative study of mountain building on an unsymmetrical earth, *J. Franklin Inst.*, *244*, 19–53, 1937.

Gunn, R., A quantitative study of isobaric equilibrium and gravity anomalies in the Hawaiian Islands, *J. Franklin Inst.*, *236*, 373–390, 1943.

Gunn, R., Quantitative aspects of juxtaposed ocean deeps, mountain chains, and volcanic ranges, *Geophysics*, *12*, 238–255, 1947.

Hanks, T. C., The Kuril Trench–Hokkaido rise system: Large shallow earthquakes and simple models of deformation, *Geophys. J. R. Astron. Soc.*, *23*, 173–189, 1971.

Haskell, N. A., The dispersion of surface waves on multilayered media, *Bull. Seismol. Soc. Am.*, *43*, 17–34, 1953.

Kirby, S. H., Tectonic stresses in the lithosphere: Constraints provided by the experimental deformation of rocks, *J. Geophys. Res.*, *85*, 6353–6363, 1980.

Louden, K. E., and D. W. Forsyth, Thermal conduction across fracture zones and the gravitational edge effect, *J. Geophys. Res.*, *81*, 4869–4874, 1976.

Mammerickx, J., Depth anomalies over Mesozoic crust in the Western Pacific, *Tectonophysics*, in press, 1982.

Mammerickx, J., and S. M. Smith, Bathymetry of the northeast Pacific, *Map and Chart Ser. MC-43*, Geol. Soc. of Am., Boulder, Colo., 1981.

McAdoo, D. C., J. G. Caldwell, and D. L. Turcotte, On the elastic-perfectly plastic bending of the lithosphere under generalized loading with application to the Kurile Trench, *Geophys. J. R. Astron. Soc.*, *54*, 11–26, 1978.

Menard, H. W., Seafloor spreading topography in the second layer, *Science*, *157*, 923–924, 1967.

Menard, H. W., and T. Atwater, Origin of fracture zone topography, *Nature, 222,* 1037–1040, 1969.

Ness, G., S. Levi, and R. Couch, Marine magnetic anomaly time scales for the Cenozoic and late Cretaceous: A précis, critique, and synthesis, *Rev. Geophys. Space Phys., 18,* 753–770, 1980.

Okal, E. A., J. Talandier, K. A. Sverdrup, and T. H. Jordan, Seismicity and tectonic stresses in the south central Pacific, *J. Geophys. Res., 85,* 6479–6495, 1980.

Oxburgh, E. R., and D. L. Turcotte, Mechanisms of continental drift, *Rep. Prog. Phys., 41,* 1249–1312, 1978.

Parker, R. L., and D. L. Oldenburg, Thermal model of ocean ridges, *Nature Phys. Sci., 242,* 137–139, 1973.

Parsons, B., and P. Molnar, The origin of outer topographic rises associated with trenches, *Geophys. J. R. Astron. Soc., 45,* 707–712, 1976.

Parsons, B., and J. G. Sclater, An analysis of the variation of ocean floor bathymetry and heat flow with age, *J. Geophys. Res., 82,* 803–827, 1977.

Reid, I., The Rivera plate: A study of seismology and plate tectonics, Ph.D. thesis, 288 pp., Univ. of Calif., San Diego, 1976.

Rowlett, I., Seismicity at intersections of spreading centers and transform faults, *J. Geophys. Res., 86,* 3815–3820, 1981.

Sibuet, J.-C., and J. Mascle, Plate kinematic implications of Atlantic equatorial fracture zone trends, *J. Geophys. Res., 83,* 3401–3421, 1978.

Turcotte, D. L., Flexure, *Adv. Geophys., 21,* 51–86, 1979.

Turcotte, D. L., D. C. McAdoo, and J. G. Caldwell, An elastic–perfectly plastic analysis of the bending of the lithosphere at a trench, *Tectonophysics, 47,* 193–206, 1978.

Van Andel, T. H., and D. Bukry, Basement ages and basement depths in the eastern equatorial Pacific from deep sea drilling project legs 5, 8, 9, and 16, *Geol. Soc. Am. Bull., 84,* 2361–2370, 1973.

Van Andel, T. H., R. P. Von Herzen, and J. D. Phillips, The Vema fracture zone and the tectonics of transverse shear zones in oceanic crustal plates, *Mar. Geophys. Res., 1,* 261–283, 1971.

Walcott, R. I., Flexure of the lithosphere at Hawaii, *Tectonophysics, 9,* 435–446, 1970.

Watts, A. B., An analysis of isostasy in the world's oceans, 1, Hawaiian-Emperor seamount chain, *J. Geophys. Res., 83,* 5989–6004, 1978.

Watts, A. B., and J. R. Cochran, Gravity anomalies and flexure of the lithosphere along the Hawaiian-Emperor seamount chain, *Geophys. J. R. Astron. Soc., 38,* 119–141, 1974.

Watts, A. B., and M. Talwani, Gravity anomalies seaward of deep sea trenches and their tectonic implications, *Geophys. J. R. Astron. Soc., 36,* 57–90, 1974.

Watts, A. B., J. H. Bodine, and M. S. Steckler, Observations of flexure and the state of stress in the oceanic lithosphere, *J. Geophys. Res., 85,* 6369–6376, 1980.

(Received July 24, 1981;
revised March 1, 1982;
accepted March 5, 1982.)